A&A 559, A125 (2013)
DOI: 10.1051/0004-6361/201322375

Astronomy & Astrophysics

The rotational spectrum of $^{12}C_2HD$ in the ground and excited bending states: an improved ro-vibrational global analysis

C. Degli Esposti[1], L. Dore[1], L. Fusina[2], and F. Tamassia[2]

[1] Dipartimento di Chimica "Giacomo Ciamician", Università di Bologna, via F. Selmi 2, 40126 Bologna, Italy
e-mail: [claudio.degliesposti;luca.dore]@unibo.it
[2] Dipartimento di Chimica Industriale "Toso Montanari", Università di Bologna, viale del Risorgimento 4, 40136 Bologna, Italy
e-mail: [luciano.fusina;filippo.tamassia]@unibo.it

Received 26 July 2013 / Accepted 11 October 2013

ABSTRACT

Rotational transitions of $^{12}C_2HD$ were recorded in the range 100–700 GHz for the vibrational ground state and for the bending states $v_4 = 1$ (Π), $v_5 = 1$ (Π), $v_4 = 2$ (Σ^+ and Δ), $v_5 = 2$ (Σ^+ and Δ), $v_4 = v_5 = 1$ (Σ^-, Σ^+ and Δ), $v_4 = 3$ (Π and Φ) and $v_5 = 3$ (Π and Φ). The transition frequencies measured in this work were fitted together with all the infrared ro-vibrational transitions involving the same bending states available in the literature. The global fit allowed a very accurate determination of the vibrational, rotational, and ℓ-type interaction parameters for the bending states up to $v_4 + v_5 = 3$ of this molecule. The results reported in this paper provide a set of information very useful for undertaking astronomical searches in both the mm−wave and the infrared spectral regions. The parameters from the global fit can be used to calculate accurate rest frequencies for rotational transitions in the ground state or in excited vibrational states involving the bending modes. Pure rotational transition frequencies up to 1 THz are listed.

Key words. molecular data – methods: laboratory: molecular – techniques: spectroscopic – catalogs

1. Introduction

Acetylene can be found in several astronomical environments: in molecular clouds (Lacy et al. 1989), in massive young stellar objects and planet forming zones (Lahuis & van Dishoeck 2000; Bast et al. 2013), in circumstellar envelopes of AGB stars (Ridgway et al. 1976; Matsuura et al. 2006; Fonfría et al. 2008), and it has been identified in cometary comae (Mumma et al. 2003) as well. This unsaturated hydrocarbon may react with radicals – atomic C, CN, and CH – to form complex molecules in starless cores (Herbst 2005), it plays a key role in the formation of circumstellar carbon chain molecules (Cherchneff & Glassgold 1993) and it is even a possible precursor of benzene in a carbon-rich PPN (Woods et al. 2002).

However, $^{12}C_2H_2$ does not have a permanent dipole moment and cannot be detected by (sub-)millimetre telescopes, therefore interstellar acetylene has been detected by observing its vibration-rotation bands. The only detectable sub-millimetre features could be those due to some *P*-branch high-*J* transitions of the $\nu_5 \leftarrow \nu_4$ difference band in the THz region (Yu et al. 2009). On the other hand, non-centrosymmetric isotopologues of acetylene, such as the subject of this paper $^{12}C_2HD$, do have a small permanent electric dipole moment. The first astronomical detection of $^{12}C_2HD$ is recent, namely it has been observed in Titan's atmosphere through the Composite InfraRed Spectrometer (CIRS) mounted on the Cassini spacecraft (Coustenis et al. 2008). From these observations it was possible to derive the D/H ratio on Titan, which was previously determined only through the transitions of the CH_4/CH_3D pair.

Molecules containing less abundant isotopes are very relevant from an astrophysical point of view. Several species containing D, ^{13}C, ^{15}N, ^{18}O, among the most important, provide a tool to assess isotopic ratios in several astronomical environments (see for instance Herbst 2003; Caselli & Ceccarelli 2012; Bézard 2009). The D/H isotopic ratio is of particular interest for several reasons. It is an important experimental constraint on the Big Bang models, as deuterium was formed in abundance only in this event. It can also provide key information on the chemical processes that lead to the formation of complex organic molecules (Sandford et al. 2001). Although the cosmic D/H ratio is of the order of magnitude of 10^{-5}, abundances of a few percent with respect to their parent species can be produced in the interstellar medium through isotopic fractionation mechanisms (Herbst 2003). It is known that in cold dense interstellar clouds D-enrichment proceeds through gas phase ion-molecule exothermic reactions, but also through gas-grain chemistry (Sandford et al. 2001). Alternative routes for achieving D-H fractionation in more energetic environments and of interest for complex molecules are: a) gas phase unimolecolar photodissociation; and b) ultraviolet photolysis in D-enriched ice mantles (Sandford et al. 2001).

Laboratory rotational spectra have been observed in the past for several monodeuterated species of acetylene, including also ^{13}C containing isotopologues (Wlodarczak et al. 1989; Matsumura et al. 1980; Cazzoli et al. 2008; Degli Esposti et al. 2013). Rotational transitions of $^{12}C_2HD$ were measured up to 418 GHz for the ground vibrational state (GS) and for the $v_4 = 1$ and $v_5 = 1$ excited states, ν_4 and ν_5 being the trans and cis bending modes, respectively (Wlodarczak et al. 1989). Pure rotational transitions in the GS up to $J'' = 10$, around 650 GHz, were observed for $^{12}C_2HD$, $H^{12}C^{13}CD$ and $H^{13}C^{12}CD$ (Cazzoli et al. 2008). In the same study, ab initio calculations were performed at various levels in order to predict the electric dipole moment for these species and the equilibrium structure of acetylene.

The calculated dipole moment does not show sizable variations upon isotopic substitution of one carbon atom, and is approximately 0.01 D for all monodeuterated isotopologues in the GS. The $\nu_5 \leftarrow \nu_4$ difference band and associated hot bands for $^{12}C_2HD$ have been recorded recently in the far-infrared (FIR) region, between 60 and 360 cm^{-1}, using the synchrotron radiation at the Canadian Light Source (Predoi-Cross et al. 2011). The same band for the H^{12}C^{13}CD and H^{13}C^{12}CD isotopologues was also detected and analysed.

As far as the infrared (IR) region is concerned, several papers have been published on $^{12}C_2HD$. The most recent are the investigations of the bending states up to $v_4 + v_5 = 3$ (Fusina et al. 2005a) and of the stretching-bending bands in the 1800–4700 cm^{-1} spectral region (Fusina et al. 2005b). In both cases the spectra were recorded by Fourier transform infrared spectroscopy (FTIR). A study of the integrated band intensities in the 25–2.5 μm window was also published (Jolly et al. 2008).

In the present paper we report on the observation of the pure rotational transitions of $^{12}C_2HD$ up to 657 GHz, that is in bands 3, 6, 7, 8 and 9 of the Atacama Large Millimeter Array (ALMA). A total of 168 transitions were assigned in the GS and in various excited vibrational bending states. The rotational lines detected in this work were fitted together with the FIR (Predoi-Cross et al. 2011) and IR lines (Fusina et al. 2005a). The spectroscopic parameters obtained from the final global fit are determined with an excellent accuracy.

The high accuracy of the millimetre- and submillimetre-wave data presented in this paper, together with the increasing sensitivity of new observation systems, such as ALMA, will favour the observation of transitions belonging to this species.

It should also be stressed that the dipole moment of $^{12}C_2HD$ is strongly enhanced by the bending vibrations. Therefore, considering that some chemically rich regions, e.g. IRC+10216 (Cernicharo et al. 2011), show a high degree of vibrational excitation, this will facilitate the detection of emission lines in the bending states ν_4 or ν_5 of $^{12}C_2HD$. In Sect. 3.1, the dipole moment variation in excited bending states is discussed.

2. Experimental details

The sample of $^{12}C_2HD$ was purchased from CDN Isotopes (98.9% purity). The rotational spectra of $^{12}C_2HD$ were observed in selected frequency regions between 100 and 700 GHz, using a source-modulation mm-wave spectrometer which employs Gunn oscillators (RPG Radiometer Physics GmbH and J. E. Carlstrom Co.) as main radiation sources covering the fundamental frequency range 75–124 GHz. Higher frequencies were generated using three different frequency multipliers (VDI – Virginia Diodes, Inc. and RPG). The Gunn oscillators were phase-locked to the suitable harmonic of the frequency emitted by a computer-controlled frequency synthesizer (Schomandl), referenced to an external rubidium frequency standard (SRS Stanford Research System). This guaranteed an absolute accuracy of ca. 20 Hz to the frequency scale. A liquid-helium-cooled InSb detector (QMC Instr. Ltd.) was employed. The Gunn oscillators were frequency modulated at 6 kHz, and the detected signals were demodulated by a lock-in amplifier tuned at twice the modulation frequency, so that the second derivative of the actual spectrum profile was detected by the computer-controlled acquisition system.

Transition frequencies were recovered from a line-shape analysis of the spectral profile (Dore 2003); their accuracy, estimated by repeated measurements, was in the range 5–30 kHz depending on the signal-to-noise ratio of the recorded lines.

The absorption cell was a 3.5 m long, 10 cm in diameter glass tube equipped with polyethylene windows. A double pass arrangement based on a wire grid polarizer and a roof mirror (Ziurys et al. 1994; Dore et al. 1999) was employed to increase the absorption path. Sample pressures of a few tens of mTorr were employed during the measurements.

3. Results and discussion

3.1. Rotational analysis

The very small dipole moment of $^{12}C_2HD$ was first determined by Matsumura et al. (1980), who performed Stark-effect measurements on the $J = 2 \leftarrow 1$ rotational transition of $^{12}C_2HD$ in the $v_4 = 1, 3$ and $v_5 = 1, 3$ states. The obtained dipole moment values are: −0.02359(5) D for $v_4 = 1$, 0.05601(9) D for $v_5 = 1$, −0.09077(26) D for $v_4 = 3$ and 0.1472(21) D for $v_5 = 3$. These experimental values led to extrapolate a GS moment of 0.01001(15) D, since the dipole moments of the $v_4 = 1$ and $v_4 = 3$ states have opposite sign with respect to that of the GS. The increase of the dipole moment values due to vibrational excitation causes a considerable intensity enhancement of the excited state rotational lines, so that their detection is much easier than expected from an evaluation of the population factors. At room temperature ($kT = 207$ cm^{-1}), the population factors are $N_4/N_0 = \exp(-518/kT) = 0.0819$ and $N_5/N_0 = \exp(-677/kT) = 0.0378$, which should reduce the intensity of the rotational lines by a factor of 12 for $v_4 = 1$ and of 26 for $v_5 = 1$. It should be noticed that the bending states are doubly degenerate. However, the factor 2, which doubles the population of $v_4 = 1$ and $v_5 = 1$, has no effect on the intensity of the rotational lines. In fact, the ℓ-type doubling removes the degeneracy of the levels and rotational transitions are allowed only within each set. On the other hand, from the experimental μ values one can calculate the following ratios: $(\mu_4/\mu_0)^2 \simeq 5.6$ and $(\mu_5/\mu_0)^2 \simeq 31$, which partly compensate the unfavourable population factors of the excited states. The intensity ratio between rotational lines in the excited bending states and in the GS can be calculated as

$$\frac{I_v}{I_0} = \left(\frac{\mu_v}{\mu_0}\right)^2 \mathrm{e}^{-E_v/kT}. \quad (1)$$

The rotational transitions in $v_4 = 1$ are expected to be less intense than those of the GS by only a factor $12/5.6 \simeq 2$, whereas the lines in $v_5 = 1$ should be even stronger than those in the GS by a factor $31/26 \simeq 1.2$. Figure 1 shows a 250 MHz frequency scan in which the $J = 5 \leftarrow 4$ transitions of $v_5 = 1$, ground, and $v_4 = 1$ states are simultaneously present. The experimental intensity ratios nicely agree with the predicted ones. Anyway, for any combination of bending vibrational quanta, the dipole moment can be calculated by applying the usual expression for the vibrational dependence

$$\mu_v = \mu_0 + \sum_i \delta\mu_i v_i \quad (2)$$

as reported in Eq. (11) of Matsumura et al. (1980). The values of the parameters $\delta\mu_i$ are: $\delta\mu_4 = -0.03360(13)$ D and $\delta\mu_5 = 0.04600(17)$ D, as given in Table 3 of the same reference. For mixed excitations of ν_4 and ν_5 there is a less significant enhancement on the dipole moment, and therefore on the intensity, since $\delta\mu_4$ and $\delta\mu_5$ have opposite sign and comparable magnitude. Indeed, only transitions in the combination $v_4 + v_5$ could be

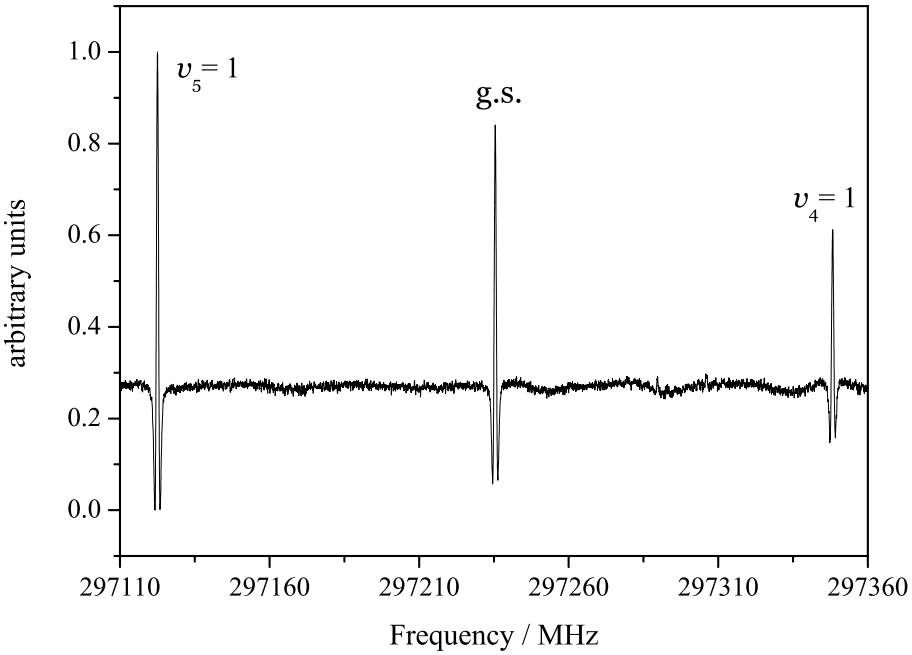

Fig. 1. The $J = 5 \leftarrow 4$ transition of $^{12}C_2HD$ in the $v_5 = 1$, ground, and $v_4 = 1$ vibrational states. The low-frequency components of each ℓ-doublet are displayed. Fourteen scans are co-added, the total integration time is 850 s.

Table 1. Dipole moments, vibrational term values, populations and intensity calculations for several excited vibrational bending states of $^{12}C_2HD$.

Vibrational state	Sym.	$\mu_v{}^a$/D	$(\mu_v/\mu_0)^2$	$E_v{}^b$/cm^{-1}	$N_v/N_0{}^c$	I_v/I_0	$N_v/N_0{}^c$	I_v/I_0
					$T = 300$ K		$T = 500$ K	
$v_4 = 1$	Π	–0.02359	5.55	518.3815	8.32×10^{-2}	4.6×10^{-1}	2.25×10^{-1}	1.2
$v_5 = 1$	Π	0.05601	31.31	677.8078	3.87×10^{-2}	1.2	1.42×10^{-1}	4.5
$v_4 = 2$	Σ^+	–0.05719	32.64	1033.9352	7.02×10^{-3}	2.3×10^{-1}	5.10×10^{-2}	1.7
$v_4 = 2$	Δ	–0.05719	32.64	1038.7208	6.86×10^{-3}	2.2×10^{-1}	5.03×10^{-2}	1.6
$v_5 = 2$	Σ^+	0.10201	103.85	1342.2266	1.60×10^{-3}	1.7×10^{-1}	2.10×10^{-2}	2.2
$v_5 = 2$	Δ	0.10201	103.85	1359.0490	1.48×10^{-3}	1.5×10^{-1}	2.00×10^{-2}	2.1
$v_4 = 3$	Π	–0.09079	82.26	1551.1573	5.88×10^{-4}	4.8×10^{-2}	1.15×10^{-2}	9.5×10^{-1}
$v_4 = 3$	Φ	–0.09079	82.26	1561.0192^d	5.61×10^{-4}	4.6×10^{-2}	1.12×10^{-2}	9.2×10^{-1}
$v_5 = 3$	Π	0.14801	218.63	2010.2240	6.50×10^{-5}	1.4×10^{-2}	3.07×10^{-3}	6.7×10^{-1}
$v_5 = 3$	Φ	0.14801	218.63	2044.0139	5.53×10^{-5}	1.2×10^{-2}	2.79×10^{-3}	6.1×10^{-1}
$v_4 = 1, v_5 = 1$	Δ	0.02241	5.01	1195.7493	3.23×10^{-3}	1.6×10^{-2}	3.20×10^{-2}	1.6×10^{-1}
$v_4 = 1, v_5 = 1$	Σ^-	0.02241	5.01	1196.1631	3.23×10^{-3}	1.6×10^{-2}	3.20×10^{-2}	1.6×10^{-1}
$v_4 = 1, v_5 = 1$	Σ^+	0.02241	5.01	1200.4983	3.16×10^{-3}	1.6×10^{-2}	3.16×10^{-2}	1.6×10^{-1}
$v_4 = 2, v_5 = 1$	$^{II}\Pi$	-0.01119	1.25	1712.1694	2.72×10^{-4}	3.4×10^{-4}	7.25×10^{-3}	9.1×10^{-3}
$v_4 = 2, v_5 = 1$	Φ	–0.01119	1.25	1715.5975	2.67×10^{-4}	3.3×10^{-4}	7.18×10^{-3}	9.0×10^{-3}
$v_4 = 2, v_5 = 1$	$^{I}\Pi$	–0.01119	1.25	1722.4715	2.58×10^{-4}	3.2×10^{-4}	7.04×10^{-3}	8.8×10^{-3}
$v_4 = 1, v_5 = 2$	$^{II}\Pi$	0.06841	46.71	1861.8584	1.32×10^{-4}	6.2×10^{-3}	4.71×10^{-3}	2.2×10^{-1}
$v_4 = 1, v_5 = 2$	Φ	0.06841	46.71	1876.5707	1.23×10^{-4}	5.8×10^{-3}	4.52×10^{-3}	2.1×10^{-1}
$v_4 = 1, v_5 = 2$	$^{I}\Pi$	0.06841	46.71	1882.4390	1.20×10^{-4}	5.6×10^{-3}	4.44×10^{-3}	2.1×10^{-1}

Notes. [a] $\mu_0 = 0.01001(15)$ D (Matsumura et al. 1980). [b] Calculated value from our global fit. [c] The population factor is calculated as $N_v/N_0 = \exp(-E_v/kT)$. [d] Calculated energy value of a state not observed experimentally in the IR spectra.

detected, whereas in higher-order mixed vibrational excitations they were too weak to be observed.

A summary of the intensity predictions at 300 K and 500 K for rotational lines of some vibrationally excited bending states is reported in Table 1. It is evident a large temperature effect, therefore at 500 K the transitions in vibrational states up to the doubly excited v_4 and v_5 are stronger than the ground-state ones.

A very limited number of excited-state transitions of $^{12}C_2HD$ have previously been observed only for $v_4 = 1, 3$ (Π) and $v_5 = 1, 3$ (Π) (Wlodarczak et al. 1989; Matsumura et al. 1980). We have considerably enlarged the previous data-set by measuring more than 150 new line frequencies, spanning J values from 1 to 10, corresponding to transitions in the ground state, in the first excited vibrational bending states $v_4 = 1$ and $v_5 = 1$ (Π), in the doubly excited $v_4 = 2$ and $v_5 = 2$ states (Σ^+ and Δ), in the combination state $v_4 = v_5 = 1$ (Σ^-, Σ^+ and Δ) and in the triply excited $v_4 = 3$ and $v_5 = 3$ states (Π and Φ). The search of the rotational lines was guided by predictions based on the spectroscopic constants determined in a previous analysis of 4888 IR and FIR data and 21 rotational transitions available at that time (Predoi-Cross et al. 2011). On average, the newly observed lines were found some hundreds of kHz away from the initial predictions. The

measured transition frequencies are listed in Table 2, along with predictions of unobserved low-J transitions and of the ones occurring at higher frequency up to 1 THz.

The term values of the observed rotational levels in the ground and excited vibrational states are in the range 2–2140 cm^{-1}. With the exception of the ground state, multiplets of rotational lines were always observed for each $J+1 \leftarrow J$ transition, because of ℓ-type resonance effects. Before performing the final ro-vibrational global analysis (see Sect. 3.2), a series of state-by-state least-squares fits were done to check the consistency of the MW measurements. The pure rotational spectra have been analysed using the formalism originally developed by Yamada et al. (1985) and already employed to fit the excited-state rotational spectra of a large number of linear carbon chains (see for example Bizzocchi & Degli Esposti 2008, and references therein). The model is slightly different from the one used to perform the global ro-vibrational analysis (see Sect. 3.2 for a detailed description), because the vibrational dependence of the various parameters is neglected, so that effective constants for each vibrational state were determined by these preliminary fits. Briefly, rotational and vibrational ℓ-type resonance effects have been treated by diagonalization of ro-vibrational matrices with off-diagonal elements which include q_t, q_t^J, $r_{tt'}$ and $r_{tt'}^J$ spectroscopic parameters (t and t' being equal to 4 or 5). The vibrational energy differences between the interacting ℓ sublevels ($\Delta\ell_t = \pm 2$) of each doubly or triply excited vibrational state have been expressed through the effective values of the constants g_{44}, g_{55} and g_{45}, which produce ℓ-dependent energy contributions. In addition, the ℓ-dependence of rotational and quartic centrifugal distortion constants have been taken into accounts trough the $\gamma^{tt'}$ and $\delta^{tt'}$ parameters, respectively. Generally, not all of the required constants can be statistically determined from the rotational transitions of a single vibrational state, and some assumptions had to be necessarily made. The ℓ-type doubling parameters q_t and q_t^J were fitted for the $v_t = 1$ ($t = 4$ or 5) and $v_t = 3$ states (where degenerate $\ell = \pm 1$ levels do exist), but constrained to interpolated values for the $v_t = 2$ states, in order to avoid high correlations with the g_{44} and g_{55} constants. The latter constant has a rather large value (ca. 5.2 cm^{-1}), so that rotational ℓ-type resonance effects are weak in the $v_5 = 3$ state, where no splitting of the $|\ell| = 3$ lines could be observed. As far as the $v_4 = v_5 = 1$ combination state is concerned, where rotational and vibrational ℓ-type resonance effects are simultaneously present, q_t and q_t^J constants were held fixed at the values determined for the singly excited bending states, while the parameters involved in the vibrational ℓ-type resonance, namely g_{45}, r_{45} and r_{45}^J were refined. The various state-by-state fits were repeated iteratively in order to achieve full consistency of the obtained parameters. The results of the eight least-squares fits performed are collected in Tables 3 and 4.

3.2. Global ro-vibrational analysis

Ro-vibrational transitions involving the vibrational states presently studied, except the $v_4 = 3$ state (Φ), were already observed in the FIR and IR regions (Predoi-Cross et al. 2011; Fusina et al. 2005b). They have been fitted together with the rotational transitions presently measured. The model Hamiltonian adopted for the global analysis represents an extension up to three quanta of the bending excitation, i.e. $v_4 + v_5 = 3$, of the Hamiltonian for a molecule with two bending vibrations which has been described in detail by Herman et al. (1991). It was already used for $^{13}C_2HD$ (Degli Esposti et al. 2013) and $^{12}C_2HD$ (Fusina et al. 2005a) itself. The term values of the ro-vibrational levels of the transitions were obtained by diagonalizing the appropriate energy matrix containing the following vibrational (G^0) and rotational (F) diagonal contributions:

$$\begin{aligned} G^0(v_4,\ell_4,v_5,\ell_5) &= \omega_4^0 v_4 + \omega_5^0 v_5 + x_{44}^0 v_4^2 + x_{45}^0 v_4 v_5 + x_{55}^0 v_5^2 \\ &+ g_{44}^0 \ell_4^2 + g_{45}^0 \ell_4 \ell_5 + g_{55}^0 \ell_5^2 \\ &+ y_{444} v_4^3 + y_{445} v_4^2 v_5 + y_{455} v_4 v_5^2 + y_{555} v_5^3 \\ &+ y_4^{44} v_4 \ell_4^2 + y_4^{45} v_4 \ell_4 \ell_5 + y_4^{55} v_4 \ell_5^2 \\ &+ y_5^{44} v_5 \ell_4^2 + y_5^{45} v_5 \ell_4 \ell_5 + y_5^{55} v_5 \ell_5^2 \end{aligned}$$

$$\begin{aligned} F(v_4,\ell_4,v_5,\ell_5) &= \Big[B_0 - \alpha_4 v_4 - \alpha_5 v_5 + \gamma_{44} v_4^2 + \gamma_{45} v_4 v_5 + \gamma_{55} v_5^2 \\ &+ \gamma^{44} \ell_4^2 + \gamma^{45} \ell_4 \ell_5 + \gamma^{55} \ell_5^2 \\ &+ \gamma_{444} v_4^3 + \gamma_{445} v_4^2 v_5 + \gamma_{455} v_4 v_5^2 + \gamma_{555} v_5^3 \\ &+ \gamma_4^{44} v_4 \ell_4^2 + \gamma_4^{45} v_4 \ell_4 \ell_5 + \gamma_4^{55} v_4 \ell_5^2 \\ &+ \gamma_5^{44} v_5 \ell_4^2 + \gamma_5^{45} v_5 \ell_4 \ell_5 + \gamma_5^{55} v_5 \ell_5^2 \Big] \Big[M - k^2\Big] \\ &- \Big[D_0 + \beta_4 v_4 + \beta_5 v_5 + \delta_{44} v_4^2 + \delta_{45} v_4 v_5 + \delta_{55} v_5^2 \\ &+ \delta^{44} \ell_4^2 + \delta^{45} \ell_4 \ell_5 + \delta^{55} \ell_5^2 \Big] \Big[M - k^2\Big]^2 \\ &+ \Big[H_0 + h_4 v_4 + h_5 v_5\Big] \Big[M - k^2\Big]^3 \end{aligned}$$

with $M = J(J+1)$ and $k = \ell_4 + \ell_5$.

Vibrational and rotational ℓ-type resonances are expressed by off-diagonal matrix elements (Herman et al. 1991) containing the following parameters:

$$\begin{aligned} r_{45} &= r_{45}^0 + r_{445}(v_4+1) + r_{455}(v_5+1) + r_{45}^J M \\ q_t &= q_t^0 + q_{tt} v_t + q_{tt'} v_{t'} + q_t^J M + q_t^{JJ} M^2 + q_t^k (k \pm 1)^2 \\ \rho_t &= \rho_t^0 + \rho_{tt} v_t + \rho_{tt'} v_{t'} + \rho_t^J M + \rho_t^{JJ} M^2 \end{aligned}$$

and

$$\rho_{45}^0 + \rho_{45}^J M.$$

The global fit included 5317 IR and 168 MW transitions. Overlapping lines were given zero weight. The uncertainty for the FIR and IR data was in the range 5.0×10^{-5}–2.0×10^{-4} cm^{-1}, and 1.0×10^{-7} cm^{-1} for the MW data. The MW blended lines were given an uncertainty of $\sqrt{2} \times 1.0 \times 10^{-7}$ cm^{-1}. Finally, 489 IR transitions, 9.2%, were excluded in the final fit because they were overlapping (271) or their observed-calculated values (218) were larger than 5 times their estimated experimental uncertainty.

For the $3\nu_4(\Phi)$ state, the $J'' = 3$ e/f components were not resolved. For the $3\nu_5(\Phi)$ state, all the e/f components of the rotational lines were not resolved. The couples of overlapping lines were identified by the same frequency (see Table 2) and their observed-calculated values were derived from the comparison of the experimental frequency with the average of the frequencies calculated for the two components. Sixty nine statistically well determined parameters, which are collected in Table 5, were refined with a final rms value of 3.06×10^{-4} cm^{-1} for the IR data and 19 kHz for the MW data. A few parameters in the model not reported in Table 5 were nevertheless allowed to vary during the fitting procedure but they resulted statistically undetermined and were constrained to zero. Some of the parameters are highly correlated, i.e. ω_4^0, x_{44}^0 and y_{444}, g_{44}^0 and y_4^{44}, γ^{44} and γ_4^{44}. The results in Table 5 can be compared with those obtained from the previous analysis, see Table 2 of Predoi-Cross et al. (2011). Sixty two parameters are common to both sets. The inclusion of the MW

Table 2. Measured and predicted[a] transition frequencies (MHz) of $^{12}C_2HD$ in the ground and excited bending states[b] .

J_{lower}	e	f	e	f
	GS(Σ^+)			
0	59 450.3568(0.5)*			
1	118 899.903(6)			
2	178 347.800(–3)[c]			
3	237 793.258(0)			
4	297 235.446(–1)			
5	356 673.553(0)			
6	416 106.758(–1)[c]			
7	475 534.251(0)[c]			
8	534 955.215(2)[c]			
9	594 368.829(–1)			
10	653 774.290(0)[c]			
11	713 170.778(6)*			
12	772 557.481(12)*			
13	831 933.589(22)*			
14	891 298.290(37)*			
15	950 650.773(58)*			
	$\nu_4(\Pi)$		$\nu_5(\Pi)$	
1	118 945.089(0)	119 477.269(9)	118 854.758(4)	119 277.533(1)
2	178 415.5619(2.6)*	179 213.7501(2.3)*	178 280.0823(1.4)*	178 914.2101(1.4)*
3	237 883.550(0)	238 947.680(8)	237 702.953(0)	238 548.385(1)
4	297 348.224(0)	298 678.175(5)	297 122.546(–1)	298 179.221(4)
5	356 808.761(4)	358 404.387(0)	356 538.043(–1)	357 805.879(4)
6	416 264.320(1)	418 125.467(–2)	415 948.623(–2)	417 427.522(–2)
7	475 714.076(–6)	477 840.554(–4)	475 353.469(–3)	477 043.325(–3)
8	535 157.215(–2)	537 548.791(–7)	534 751.765(1)	536 652.447(–8)
9	594 592.901(3)	597 249.321(–14)	594 142.692(9)	596 254.063(3)
10	654 020.294(9)*	656 941.326(15)	653 525.403(–6)	655 847.322(3)
11	713 438.577(13)*	716 623.870(8)*	712 899.122(5)*	715 431.393(5)*
12	772 846.920(18)*	776 296.158(12)*	772 263.004(7)*	775 005.447(7)*
13	832 244.493(25)*	835 957.316(16)*	831 616.236(10)*	834 568.646(10)*
14	891 630.469(32)*	895 606.491(21)*	890 957.998(13)*	894 120.156(13)*
15	951 004.018(41)*	955 242.824(28)*	950 287.470(17)*	953 659.140(17)*
	$2\nu_4(\Sigma^+)$		$2\nu_4(\Delta)$	
1	119 546.034(2)			
2	179 263.6778(1.3)*		179 309.3350(1.8)*	179 275.7267(1.3)*
3	239 060.981(4)		239 044.331(4)	239 014.204(6)
4	298 797.083(4)		298 821.521(5)	298 761.253(–4)
5	358 513.791(1)		358 609.405(0)	358 503.985(–3)
6	418 207.331(–3)		418 410.034(1)	418 241.519(–7)
7	477 874.064(–4)		478 225.308(3)	477 973.005(–1)
8	537 510.557(–9)		538 056.907(0)	537 697.560(–3)
9	597 113.735(9)		597 906.201(–3)	597 414.336(6)
10	656 680.889(6)*		657 774.119(5)*	657 122.442(5)*
11	716 209.964(9)*		717 661.002(8)*	716 821.035(8)*
12	775 699.553(12)*		777 566.514(10)*	776 509.241(11)*
13	835 149.038(16)*		837 489.535(13)*	836 186.197(14)*
14	894 558.632(21)*		897 428.114(17)*	895 851.036(18)*
15	953 929.360(26)*		957 379.488(21)*	955 502.892(23)*
	$2\nu_5(\Sigma^+)$		$2\nu_5(\Delta)$	
1	119 266.026(–2)			
2	178 810.6120(2.1)*		178 895.5763(2.9)*	178 812.7892(2.1)*
3	238 520.965(0)		238 415.696(–2)	238 410.266(12)
4	298 140.805(–1)		298 017.458(11)	298 006.559(2)
5	357 753.710(–1)		357 617.725(–22)	357 598.691(4)
6	417 358.294(1)		417 216.318(7)	417 185.812(3)
7	476 953.162(0)		476 812.837(–13)	476 767.084(–3)
8	536 536.935(4)		536 407.080(4)	536 341.685(–4)
9	596 108.209(–3)		595 998.702(5)	595 908.779(2)
10	655 665.623(10)*		655 587.422(9)*	655 467.519(9)*
11	715 207.784(15)*		715 172.952(13)*	715 017.079(13)*

Notes. [(a)] Predicted transition frequencies are marked with *. [(b)] Observed – calculated values in kHz are in parentheses. For predicted transitions, 1σ uncertainty values in kHz are in parentheses. [(c)] From Cazzoli et al. (2008). [(d)] Blended e and f components. See text for details about the fit.

Table 2. continued.

$J_{\rm lower}$	e	f	e	f
12	774 733.323(20)*		774 754.988(17)*	774 556.623(17)*
13	834 240.875(27)*		834 333.204(23)*	834 085.316(23)*
14	893 729.088(36)*		893 907.288(29)*	893 602.322(29)*
15	953 196.627(45)*		953 476.896(37)*	953 106.809(37)*
	$\nu_4 + \nu_5(\Sigma^+)$	$\nu_4 + \nu_5(\Sigma^-)$	$\nu_4 + \nu_5(\Delta)$	
1	119 372.9313(3.1)*	119 376.714(15)		
2	179 063.7837(4.2)*	179 063.2816(4.3)*	179 051.0189(3.9)*	179 059.2583(3.9)*
3	238 758.286(–1)	238 749.345(–3)	238 719.510(25)	238 740.079(–1)
4	298 459.479(0)	298 432.869(–8)	298 374.940(1)	298 416.109(–2)
5	358 168.361(3)	358 113.842(–7)	358 014.181(4)	358 086.157(–11)
6	417 886.383(25)	417 791.720(–4)	417 634.055(–1)	417 749.085(–1)
7	477 614.796(–16)	477 465.935(–11)	477 231.522(–16)	477 403.712(–12)
8	537 354.882(–7)	537 135.893(12)	536 803.766(3)	537 048.998(18)
9	597 107.532(13)*	596 800.904(13)*	596 348.035(14)*	596 683.802(14)*
10	656 873.375(20)*	656 460.282(19)*	655 862.062(21)*	656 307.208(21)*
11	716 652.658(27)*	716 113.214(27)*	715 343.880(29)*	715 918.291(28)*
12	776 445.151(37)*	775 758.809(35)*	774 792.016(39)*	775 516.237(38)*
13	836 250.079(48)*	835 396.085(46)*	834 205.536(50)*	835 100.324(48)*
14	896 066.087(60)*	895 023.967(57)*	893 584.090(63)*	894 669.917(60)*
15	955 891.224(74)*	954 641.305(69)*	952 927.922(77)*	954 224.462(72)*
	$3\nu_4(\Pi)$		$3\nu_4(\Phi)$	
1	119 333.0966(2.5)*	120 417.290(–1)		
2	178 994.7108(3.4)*	180 620.8207(3.4)*		
3	238 650.439(–3)	240 818.166(3)	239 596.144(5)[d]	239 596.144(5)[d]
4	298 298.393(1)	301 007.179(3)	299 496.549(4)	299 497.179(–6)
5	357 936.717(–1)	361 185.646(–4)	359 397.880(–4)	359 399.589(–3)
6	417 563.648(5)	421 351.288(2)	419 300.076(–8)	419 303.924(–10)
7	477 177.470(–1)	481 501.676(–4)	479 203.105(19)	479 210.812(15)
8	536 776.594(–1)	541 634.304(3)	539 106.728(–9)	539 120.888(–5)
9	596 359.515(11)*	601 746.476(11)*	599 010.788(11)*	599 035.080(12)*
10	655 924.840(17)*	661 835.367(17)*	658 914.861(17)*	658 954.378(19)*
11	715 471.300(26)*	721 897.959(25)*	718 818.479(25)*	718 879.984(29)*
12	774 997.751(36)*	781 931.046(37)*	778 721.028(35)*	778 813.287(44)*
13	834 503.177(49)*	841 931.225(52)*	838 621.766(48)*	838 755.872(64)*
14	893 986.690(65)*	901 894.902(74)*	898 519.824(64)*	898 709.517(90)*
15	953 447.530(84)*	961 818.305(103)*	958 414.206(83)*	958 676.176(126)*
	$3\nu_5(\Pi)$		$3\nu_5(\Phi)$	
1	119 009.261(–9)	119 878.115(5)		
2	178 511.2975(4.1)*	179 814.4690(4.1)*		
3	238 010.190(–8)	239 747.595(4)	238 645.147(–2)[d]	238 645.147(–2)[d]
4	297 504.944(12)	299 676.394(0)	298 301.690(2)[d]	298 301.690(2)[d]
5	356 994.448(–13)	359 599.794(2)	357 955.058(–5)[d]	357 955.058(–5)[d]
6	416 477.774(23)	419 516.690(–5)	417 604.645(2) [d]	417 604.645(2) [d]
7	475 953.761(–10)	479 426.001(–9)	477 249.801(6) [d]	477 249.801(6) [d]
8	535 421.492(–1)	539 326.646(8)	536 889.885(–4) [d]	536 889.885(–4) [d]
9	594 879.894(13)*	599 217.473(13)*	596 523.777(13)*	596 524.816(14)*
10	654 327.955(20)*	659 097.403(20)*	656 151.543(20)*	656 153.234(21)*
11	713 764.666(29)*	718 965.307(29)*	715 772.221(29)*	715 774.853(31)*
12	773 189.019(40)*	778 820.056(40)*	775 385.140(40)*	775 389.093(43)*
13	832 600.016(53)*	838 660.512(53)*	834 989.623(53)*	834 995.380(58)*
14	891 996.663(69)*	898 485.527(68)*	894 584.987(68)*	894 593.151(75)*
15	951 377.978(87)*	958 293.939(86)*	954 170.539(86)*	954 181.857(95)*

data allowed the determination of 7 additional constants. Three of these are related to the ν_4 bending states, partly because experimental data for the $v_4 = 3(\Phi)$ state have been obtained for the first time. Values and signs of all the common parameters are consistent in both sets: the differences between new and old values being in the range 0–1% (31 parameters), 1–10% (18 parameters), 10–50% (7 parameters), 50–100% (5 parameters) and 1 parameter, h_4, differs by 306%. The inclusion of the MW data also yields a significant improvement of the precision of the main constants which contribute to the rotational energy. For example, the values of B_0, α_t, and q_t^0 constants are ca. 5 times more precise than those determined previously (Predoi-Cross et al. 2011). It should be pointed out that in the present global analysis 60 additional IR transitions were discarded in the final fit, compared with the previous fit (Predoi-Cross et al. 2011), adopting the same rejection limits. The discarded lines are scattered over most of the bands. Considering the high accuracy of the assigned MW transitions, this result is particularly pleasing since

Table 3. Effective spectroscopic constants determined from state-by-state fits of the rotational transitions measured for the ground and $v_4 = 1$, $v_5 = 1$, $v_4 = v_5 = 1$ states of $^{12}C_2HD$[a].

Parameter	Unit	*G.S.*	$v_4 = 1$	$v_5 = 1$	$v_4 = v_5 = 1$
B	MHz	29725.24646(27)	29805.44743(32)	29770.36999(18)	29849.79104(50)
Previous value		29725.24501(82)[b]	29803.0066(43)[c]	29766.7458(44)[c]	
D	kHz	34.0383(41)	35.1929(21)	34.5408(10)	35.5450(43)
Previous value		34.0186(45)[b]	35.107(44)[c]	34.482(54)[c]	
H	Hz	0.090(18)			
γ^{44}	MHz		–2.44328[d]		–2.44328[d]
δ^{44}	kHz		–0.1003 [d]		
γ^{55}	MHz			–3.62753[d]	–3.62753[d]
δ^{55}	kHz			–0.0767 [d]	
γ^{45}	MHz				0.07645(52)
q_t	MHz		133.05208(66)	105.69975(36)	[e]
Previous value			133.0259(71)[c]	105.6843(65)[c]	
q_t^J	kHz		–1.1512(42)	-0.6544(21)	[f]
Previous value			–1.205(26)[c]	–0.693(24)[c]	
g_{45}	GHz				20.9453(26)
r_{45}	GHz				64.5713(27)
r_{45}^J	MHz				–0.72846(35)
$\sigma_{\rm fit}$	kHz	2.9	7.5	4.4	12.5
No. of lines		10	17	18	25
J range		1–10	1–10	1–10	1–8

Notes. [(a)] Estimated uncertainties (1σ) are given in parentheses in units of the last figure quoted. [(b)] From Cazzoli et al. (2008). [(c)] From Wlodarczak et al. (1989). [(d)] Fixed in the analysis at the value extrapolated from the doubly and triply excited bending states. [(e)] q_4 and q_5 fixed in the analysis at the values determined for the singly excited bending states. [(f)] q_4^J and q_5^J fixed in the analysis at the values determined for the singly excited bending states.

Table 4. Effective spectroscopic constants determined from state-by-state fits of the rotational transitions measured for the $v_4 = 2$, $v_4 = 3$, $v_5 = 2$ and $v_5 = 3$ states of $^{12}C_2HD$[a].

Parameter	Unit	$v_4 = 2$	$v_4 = 3$	$v_5 = 2$	$v_5 = 3$
B	MHz	29887.55176(34)	29971.53551(53)	29816.92379(54)	29864.91215(61)
Previous value			29969.052(43)[c]		29861.189(27)[c]
D	kHz	36.3586(26)	37.470(20)	35.0859(42)	35.6706(42)
γ^{44}	MHz	–2.47788(10)	–2.512476(79)		
δ^{44}	kHz	–0.07435(86)	–0.0484(39)		
γ^{55}	MHz			–3.70183(17)	–3.77613(11)
δ^{55}	kHz			–0.0767(14)	–0.0767[b]
q_t	MHz	134.29328[b]	135.53447(47)	107.15528[b]	108.61081(56)
Previous value			135.529(25)[c]		108.642(28)[c]
q_t^J	kHz	–1.2082[b]	–1.2653(44)	–0.6905[b]	–0.7267(47)
g_{44}	GHz	65.82005(36)	67.137(12)		
g_{55}	GHz			156.406(11)	158.484(62)
σ_{fit}	kHz	5.0	8.0	8.1	10.0
No. of lines		22	24	22	20
J range		1–9	1–8	1–9	1–8

Notes. [(a)] Estimated uncertainties (1σ) are given in parentheses in units of the last figure quoted. [(b)] Fixed in the analysis. See text. [(c)] From Matsumura et al. (1980).

it confirms the validity of the calibration of the IR data, which span a wide wavenumber range, from about 90 to 2100 cm^{-1}.

4. Conclusions

Rotational lines of $^{12}C_2HD$ were detected in the range 100–700 GHz. They were analysed together with the IR transitions reported in the literature in a global fit. Sixty nine parameters (rotational, vibrational, ro-vibrational, and ℓ-type interaction) were determined with high precision. The analysis of the ℓ-type resonances which affect the pure rotational spectra allows the determination of the small vibrational energy differences ΔG between different ℓ-sublevels of a given vibrational state, which can be directly calculated using the effective values of the fitted $g_{tt'}$, r_{45} and B_v constants in Tables 3 and 4. The reliability of these results can be checked by comparison with the corresponding values from the global analysis. Table 6 shows that the agreement between the two sets of ΔG values is very good, differences being mostly less than one percent, thus confirming that an accurate treatment of ℓ-type resonances in the pure rotational spectra can provide precise information on the vibrational energy. The set of spectroscopic constants determined in this work is the most accurate and consistent available in the literature. From these constants it is possible to derive very accurate predictions for IR and MW spectra useful for astronomical searches. An extensive list

Table 5. Spectroscopic parameters (in cm^{-1}) for the bending states of $^{12}C_2HD$ resulting from the simultaneous fit of all rovibrational and rotational transitions involving levels up to $v_4 + v_5 = 3^a$.

Parameter		Parameter	
ω_4^0	517.402601(218)	g_{44}^0	2.115710(164)
ω_5^0	676.1872194(422)	g_{45}^0	0.8520559(414)
x_{44}^0	–0.145264(162)	g_{55}^0	5.1617199(204)
x_{45}^0	0.7073464(602)	y_4^{44}	0.0386452(816)
x_{55}^0	–2.5974827(345)	y_4^{45}	–0.1020513(272)
y_{444}	–0.0361132(273)	y_4^{55}	0.0220361(276)
y_{555}	0.03026153(794)	y_5^{44}	0.0399687(352)
y_{455}	0.0425917(215)	y_5^{45}	–0.0497444(235)
y_{445}	0.0427392(230)	y_5^{55}	0.01898570(786)
r_{45}^0	1.558537(256)	r_{445}	0.066625(144)
r_{455}	0.2376927(666)	$r_{45}^J \times 10^3$	–0.02425307(715)
B_0	0.99152746042(798)	$\gamma^{44} \times 10^3$	–0.0803231(111)
$\alpha_4 \times 10^3$	–2.6433354(162)	$\gamma^{45} \times 10^3$	–0.002734(103)
$\alpha_5 \times 10^3$	–1.4813042(109)	$\gamma^{55} \times 10^3$	–0.11852215(598)
$\gamma_{44} \times 10^3$	0.0320827(114)	$\gamma_4^{44} \times 10^6$	–1.15751(389)
$\gamma_{45} \times 10^3$	–0.0254007(772)	$\gamma_4^{45} \times 10^6$	2.4004(700)
$\gamma_{55} \times 10^3$	0.02386750(325)	$\gamma_4^{55} \times 10^6$	–0.5481(311)
$\gamma_{444} \times 10^6$	–0.13205(272)	$\gamma_5^{44} \times 10^6$	–2.4642(524)
$\gamma_{445} \times 10^6$	2.0608(324)	$\gamma_5^{45} \times 10^6$	2.9034(567)
$\gamma_{455} \times 10^6$	0.2960(296)	$\gamma_5^{55} \times 10^6$	–2.47508(202)
$D_0 \times 10^6$	1.1348569(460)	$\delta_{55} \times 10^9$	0.3352(113)
$\beta_4 \times 10^6$	0.0360515(446)	$\delta^{44} \times 10^9$	–1.0216(230)
$\beta_5 \times 10^6$	0.0166603(420)	$\delta^{45} \times 10^9$	1.0568(731)
$\delta_{44} \times 10^9$	–0.6920(160)	$\delta^{55} \times 10^9$	–2.0961(255)
$H_0 \times 10^{12}$	1.0517(533)	$h_5 \times 10^{12}$	0.2711(170)
$h_4 \times 10^{12}$	0.8211(213)		
$q_4^0 \times 10^3$	4.3971804(145)	$q_4^J \times 10^6$	–0.0396014(590)
$q_5^0 \times 10^3$	3.4775451(139)	$q_5^J \times 10^6$	–0.0229481(559)
$q_{44} \times 10^3$	0.04117559(416)	$q_4^{JJ} \times 10^{12}$	0.3843(367)
$q_{45} \times 10^3$	–0.0055881(646)	$q_5^{JJ} \times 10^{12}$	0.3524(376)
$q_{54} \times 10^3$	0.0177668(890)	$q_5^k \times 10^6$	–5.0405(982)
$q_{55} \times 10^3$	0.04839697(402)		
$\rho_4^0 \times 10^6$	–0.016295(311)	$\rho_{55} \times 10^9$	8.740(197)
$\rho_5^0 \times 10^6$	–0.018320(392)	$\rho_4^J \times 10^{12}$	–3.082(119)
$\rho_{44} \times 10^9$	3.844(155)	$\rho_5^J \times 10^{12}$	–0.6290(815)
$\rho_{45}^0 \times 10^9$	–1.744(191)		
Number of IR data fitted		4828	
Number of MW data fitted		168	
St. dev. of the IR data/ $cm^{-1} \times 10^4$		3.06	
St. dev. of the MW data/kHz		19	

Notes. [(a)] Estimated uncertainties (1σ) are given in parentheses in units of the last figure quoted.

Table 6. Vibrational energy differences (cm^{-1}) between ℓ-sublevels of doubly and triply excited bending states of $^{12}C_2HD$, as resulting from the rotational analysis and the global rovibrational analysis.

Vibrational state	sublevels	ΔG rotational analysis	ΔG global analysis
$v_4 = 2$	$\Delta - \Sigma^+$	8.782	8.772
$v_4 = 3$	$\Phi - \Pi$	17.916	17.544
$v_5 = 2$	$\Delta - \Sigma^+$	20.868	20.799
$v_5 = 3$	$\Phi - \Pi$	42.280	41.598
$v_4 = v_5 = 1$	$\Delta - \Sigma^+$	1.397	1.401

of rotational frequencies up to 1 THz is reported in Table 2 for all the observed vibrational states, whose energies are reported in Table 1. The line strength of each transition can be calculated by the simple formula (Lafferty & Lovas 1978):

$$S(J+1 \leftarrow J) = \frac{(J+1)^2 - \ell^2}{(J+1)}. \quad (3)$$

Acknowledgements. The authors acknowledge the Università di Bologna and the Ministero della Ricerca e dell'Università for financial support under the grant PRIN09 "High-resolution Spectroscopy for Atmospherical and Astrochemical Research: Experiment, Theory and Applications". The authors also thank Prof. G. Di Lonardo for helping the analysis of the infrared spectra.

References

Bast, J. E., Lahuis, F., van Dishoeck, E. F., & Tielens, A. G. G. M. 2013, A&A, 551, A118
Bézard, B. 2009, Phil. Trans. Roy. S. London, Ser. A, 367, 683
Bizzocchi, L., & Degli Esposti, C. 2008, Chem. Phys., 346, 139
Caselli, P., & Ceccarelli, C. 2012, A&AR, 20, 56
Cazzoli, G., Puzzarini, C., Fusina, L., & Tamassia, F. 2008, J. Mol. Spectr., 247, 115
Cernicharo, J., Agúndez, M., Kahane, C., et al. 2011, A&A, 529, L3
Cherchneff, I., & Glassgold, A. E. 1993, ApJ, 419, L41
Coustenis, A., Jennings, D. E., Jolly, A., et al. 2008, Icarus, 197, 539
Degli Esposti, C., Dore, L., Fusina, L., & Tamassia, F. 2013, Mol. Phys., 111, 896
Dore, L. 2003, J. Mol. Spectr., 221, 93

Dore, L., Degli Esposti, C., Mazzavillani, A., & Cazzoli, G. 1999, Chem. Phys. Lett., 300, 489
Fonfría, J. P., Cernicharo, J., Richter, M. J., & Lacy, J. H. 2008, ApJ, 673, 445
Fusina, L., Canè, E., Tamassia, F., & Lonardo, G. D. 2005a, Mol. Phys., 103, 3263
Fusina, L., Tamassia, F., & Lonardo, G. D. 2005b, Mol. Phys., 103, 2613
Herbst, E. 2003, Space Sci. Rev., 106, 293
Herbst, E. 2005, J. Phys. Chem. A, 109, 4017
Herman, M., Huet, T., Kabbadj, Y., & Auwera, J. V. 1991, Mol. Phys., 72, 75
Jolly, A., Benilan, Y., Canè, E., et al. 2008, J. Quant. Spectr. Rad. Transf., 109, 2846
Lacy, J. H., Evans, II, N. J., Achtermann, J. M., et al. 1989, ApJ, 342, L43
Lafferty, W. J., & Lovas, F. J. 1978, J. Phys. Chem. Ref. Data, 7, 441
Lahuis, F., & van Dishoeck, E. F. 2000, A&A, 355, 699
Matsumura, K., Tanaka, T., Endo, Y., Saito, S., & Hirota, E. 1980, J. Phys. Chem., 84, 1793
Matsuura, M., Wood, P. R., Sloan, G. C., et al. 2006, MNRAS, 371, 415
Mumma, M., DiSanti, M., Russo, N. D., et al. 2003, Adv. Space Res., 31, 2563
Predoi-Cross, A., Herman, M., Fusina, L., & Lonardo, G. D. 2011, Mol. Phys., 109, 559
Ridgway, S. T., Hall, D. N. B., Wojslaw, R. S., Kleinmann, S. G., & Weinberger, D. A. 1976, Nature, 264, 345
Sandford, S. A., Bernstein, M. P., & Dworkin, J. P. 2001, MAPS, 36, 1117
Wlodarczak, G., Demaison, J., Burie, J., & Lasne, M. C. 1989, Mol. Phys., 66, 669
Woods, P. M., Millar, T. J., Zijlstra, A. A., & Herbst, E. 2002, ApJ, 574, L167
Yamada, K. M., Birss, F., & Aliev, M. 1985, J. Mol. Spectr., 112, 347
Yu, S., Drouin, B. J., & Pearson, J. C. 2009, ApJ, 705, 786
Ziurys, L., Jr., W. B., Anderson, M., Fletcher, D., & Lamb, J. 1994, Rev. Sci. Instrum., 65, 1517